Regulatory mechanisms of the mucin-like region on herpes simplex virus during cellular attachment.

[a]*Martin Delguste*[+], [b]*Nadia Peerboom*[+], [a]*Grégoire Le Brun*, [c]*Edward Trybala*, [c]*Sigvard Olofsson*, [c]*Tomas Bergström*, [a]*David Alsteens**,[d,e]*Marta Bally**

[a] *Louvain Institute of Biomolecular Science and Technology, UCLouvain, 1348 Louvain-la-Neuve, Belgium*

[b] *Department of Physics, Chalmers University of Technology, 41296 Göteborg, Sweden*

[c] *Department of Infectious Diseases, University of Gothenburg, 41346 Göteborg, Sweden*

[d] *Department of Clinical Microbiology, Umeå University, 90185 Umeå, Sweden*

[e] *Wallenberg Centre for Molecular Medicine, Umeå University, 90185 Umeå, Sweden*

[+] These authors contributed equally to this work

* Contributed equally. To whom correspondence should be addressed: david.alsteens@uclouvain.be; marta.bally@umu.se

Abstract

Mucin-like regions, characterized by a local high density of O-linked glycosylation, are found on the viral envelope glycoproteins of many viruses. Herpes simplex virus type 1 (HSV-1), for example, exhibits a mucin-like region on its glycoprotein gC, a viral protein involved in initial recruitment of the virus to the cell surface via interaction with sulfated glycosaminoglycans. So far, this mucin-like region has been proposed to play a key role in modulating the interactions with cellular glycosaminoglycans, and in particular to promote release of HSV-1 virions from infected cells. However, the molecular mechanisms and its role as a pathogenicity factor remain unclear. Using single virus particle tracking we show that the mobility of chondroitin sulfate-bound HSV-1 virions is decreased in absence of the mucin-like region. This decrease in mobility correlates with an increase in HSV-1-chondroitin sulfate binding forces as observed using atomic force microscopy-based force spectroscopy. Our data suggests that the mucin-like region modulates virus-glycosaminoglycan interactions by regulating the affinity, type and number of glycoproteins involved in virus-glycosaminoglycan interaction. This study therefore presents new evidence for a role of the mucin-like region in balancing the interaction of HSV-1 with glycosaminoglycans, and provides further insights into the molecular mechanisms used by the virus to ensure both successful cell entry and release from the infected cell.

Many viruses take advantage of their host cell glycosylation pathways for modification of the viral proteins. Accordingly, viral envelope glycoproteins present structures resembling those of cell-surface glycans, consisting of N-linked or O-linked oligosaccharides [1-2]. It is believed that an important role of these glycan structures is to protect the virus from the host immune response, which more easily tolerates self-like structures [2-4]. Furthermore, these protein modifications have been shown to promote proper folding of the viral glycoproteins, thereby ensuring their functionality [2].

Glycan structures are rarely uniformly distributed along the viral glycoproteins, but can form clusters of heavily glycosylated domains. For example, certain glycoproteins have been found to comprise regions of numerous clustered O-linked glycans, which structurally resemble the heavily glycosylated sequences of mucins [5]. These so-called mucin-like regions (MLRs) form extended hydrophilic domains, which can cover substantial parts of the underlying protein structure [6]. They have been found on glycoproteins of a number of different viruses, such as the herpes simplex virus (HSV), respiratory syncytial virus, human immunodeficiency virus, Ebola virus or Marburg virus [2-3, 6].

This study focuses on the role of the MLR located at the N-terminal part of attachment glycoprotein C (gC) of HSV-1 in regulating attachment and release of HSV-1 to and from cell-surface glycosaminoglycans (GAGs), the main attachment targets for HSV [7-8]. We recently suggested that this mucin-like domain balances the interactions of HSV-1 with GAGs to ensure successful release of progeny virions from the surface of infected cells. This hypothesis was based on two observations [9]: First, cell infection with viral mutants lacking the MLR resulted in a >20 fold decrease in spontaneously released virions from the cell surface. Second, purified gC proteins lacking the MLR did not show any detectable dissociation from surface-bound GAGs, unlike their native variants. While our previous study provided evidence for a role of the MLR in balancing the interactions of HSV-1 with cell-surface GAGs, further investigations are needed to understand the function of these glycan structures and the underlying mechanisms.

The aim of this study was to elucidate the influence of the MLR of glycoprotein gC on the characteristics of virus-GAG interactions. To this end, we studied the binding behavior of single HSV-1 particles to chondroitin sulfate (CS), a GAG found at the cell surface and known to interact with HSV [8, 10]. The results were compared to an escape mutant HSV-1 strain selected by serial passage with the GAG-mimetic muparfostat and lacking the MLR on gC [9, 11]. Single particle tracking (SPT) yields quantitative information on the influence of protein glycosylation on the diffusive behavior of GAG-bound virions. Additionally, force-distance curve (FD)-based atomic force microscopy (AFM) was used to characterize interaction forces between virus and GAGs while an ELISA-based assay [12] allowed us to further investigate the accessibility of various glycoproteins in the virus envelope.

Results and Discussion

HSV-1 mutants lacking the mucin-like region on gC show decreased mobility on CS

We previously reported that HSV-1 virions can undergo lateral diffusion when bound to CS chains end-grafted to a solid substrate [10] and that the MLR affects the attachment and detachment behavior of HSV-1 virions [9]. We therefore proceeded with investigating whether the MLR also affects the diffusive behavior of HSV-1 on GAGs. To this end, time-lapse movies of single fluorescently labeled virus particles were recorded using total internal reflection fluorescence microscopy (TIRFM); SPT analysis was performed to estimate diffusion coefficients from individual particle trajectories (**Figure 1a**). The diffusive behavior of a mutant HSV-1 virion lacking the MLR on gC (KOSc-gCΔmuc) was compared to our previously published data on WT [10]. Our analysis revealed that KOSc-gCΔmuc virions, like their wild-type variants undergo either normal or anomalous diffusion. For the KOSc-gCΔmuc virus, 14.1% ± 3% of all tracks could be assigned to anomalous diffusion, which was possibly slightly lower (p-value =0.06) than for the WT virus (21.9% ± 5.3%). For both diffusion modes, the histograms of diffusion coefficients showed two distinct peaks (**Figure 1b and Table 1**). The first one, at a D value of ~ 10^{-6} $\mu m^2/s$ for anomalous diffusion and ~ 10^{-8} $\mu m^2/s$ for normal diffusion, was assigned to immobile particles where the nonzero D values are related to the localization noise. [10] In addition, a second peak, assigned to mobile particles appeared at ~ 10^{-3} $\mu m^2/s$ for anomalous diffusion and ~ 10^{-6} $\mu m^2/s$ for normal diffusion, i.e. 2-3 orders of magnitude higher than the immobile peak.

To compare the diffusive behavior of the KOSc-gCΔmuc virus to the wild-type strain, we calculated mobile fractions (# mobile particles / # particles) for both diffusion modes combined. We found that the mobile fraction of the KOSc-gCΔmuc virus was significantly decreased as compared to the wild-type strain (**Figure 1c**), thereby indicating that the presence of the MLR on gC influences the diffusive properties of GAG-bound HSV-1.

Lateral diffusion of individual CS-bound HSV-1 particles has been hypothesized to mainly originate from a lateral hopping movement caused by the disruption and reformation of single HSV-CS bonds. [10] In such a case, the mobility of the virus is likely to be influenced by the number of individual ligand-receptor bonds (formed between viral glycoproteins and surface-bound CS), as well as by their respective affinities. Deletion of the MLR on gC may therefore have consequences on both of the above stated properties of the multivalent HSV-GAG interaction by directly affecting the affinity of the gC-CS interaction, or by inducing a change in the contributions from individual glycoproteins to the overall interaction (for example glycoprotein B (gB), besides gC), or by a combination of both.

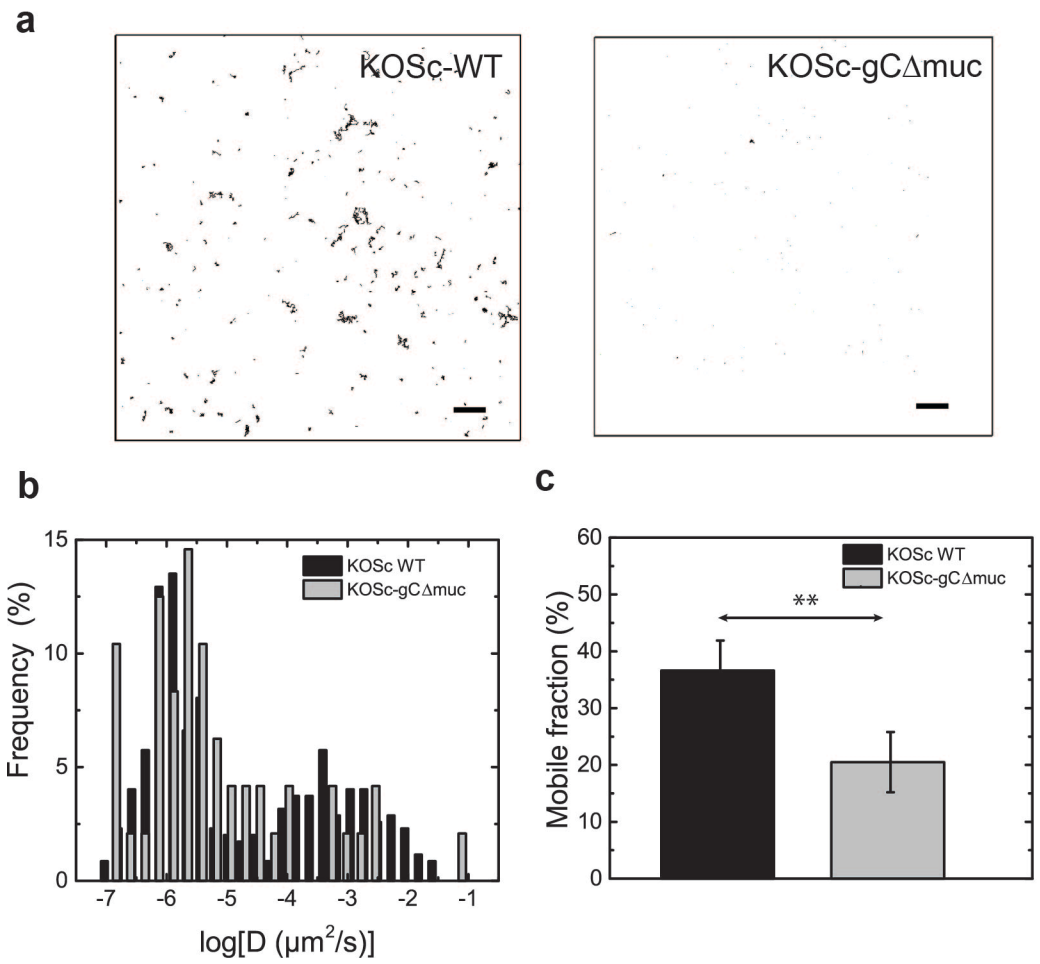

Figure 1: Single particle tracking of mutant HSV-1 particles lacking the MLR on gC (KOSc-gCΔmuc) compared to the wild-type strain (For WT see also [10]). (a) Representative image of individual tracks of HSV-1 KOSc WT (left) and KOSc-gCΔmuc (right) particles on end-grafted CS (scale bars 10 μm). (b) Histogram of diffusion coefficients (anomalous diffusion) comparing

the two virus strains for a representative dataset. (c) Average mobile fractions (with standard deviations from independent experiments ($n \geq 3$; both diffusion modes combined). Significant shifts (**p<0.01) are indicated.

Table 1: Comparison of average peak diffusion coefficients (D values, determined by log-normal Gaussian fitting of the histograms) and combined mobile fractions (# particles in mobile peaks (anomalous & normal diffusion)/ # particles) for the two virus strains ($n \geq 3$).

	Anomalous Diffusion		Normal Diffusion		
	D (10^{-6} μm^2/s) Immobile Peak	D (10^{-4} μm^2/s) Mobile Peak	D (10^{-8} μm^2/s) Immobile Peak	D (10^{-6} μm^2/s) Mobile Peak	Mobile fraction (%)
KOSc WT[10]	1.1 ± 0.2	7.9 ± 4.8	5.3 ± 0.7	8.42 ± 2.9	36.6 ± 5.3
KOSc-gCΔmuc	1.4 ± 0.6	8.4 ± 4.7	5.6 ± 1.9	0.8 ± 0.5	20.5 ± 5.3

HSV-1 mutants lacking the MLR on gC show increased binding forces with CS

To further pinpoint the molecular mechanisms underlying the influence of MLR on virus diffusion, we further performed FD-based AFM measurements using an AFM tip derivatized with a single virus particle on its apex using an optimized protocol relying on low linker densities and and appropriate virus concentration. [13] The functionalized tip is then approached onto and retracted from a surface carrying CS molecules to characterize the virus-GAG interaction. Here, HSV-1 particles were covalently attached to the AFM tips by means of a ~9 nm polyethylene glycol chain [13-16] which confers the virus local mobility and ensures reorientation for unhindered interactions with the GAGs while providing an unambiguous signature for virus-GAG interactions as the trance should be fittable with a worm- like chain model [17] describing the extension of the linker and the adhesion event should be located at ~9nm from the tip-surface contact point. The CS-chains were immobilized onto a solid substrate via their reducing end [18]. (Figure 2A). Upon retraction of the AFM tip, the binding strength is recorded.

In these experiments, FD-curves showing characteristic adhesion events on the retraction curve (see insert in **Figure 2a**) were evaluated for specificity by fitting the adhesion peak with the worm-like chain model [17] describing the elongation of the polymer chain under an applied force. Our results revealed that, on average, ~ 3.4% of the obtained curves for KOSc WT, and ~ 4.3% of the

KOSc-gCΔmuc curves showed distinguishable specific adhesion events (> 45 pN) upon retraction. The specificity of these binding events was confirmed by two independent controls: (*i*) injection of free heparin, acting as a blocking agent resulted in a > 4 fold reduction in the binding frequencies; (*ii*) when CS was replaced with the non-sulfated GAG hyaluronan (HA) the binding frequencies were reduced to ~ 1.1%. (See also adhesion maps in **Suppl. Fig. 1**) Together, these controls confirmed that the recorded binding events originated from the tip-bound HSV-1 virion interacting with CS.

Next, for each individual specific adhesive peak on *FD*-curves, we extracted the binding force (F), representing the force needed to disrupt the virus-GAG interaction, together with the loading rate (LR, increase of the force applied to the bond over time) from the force *vs* time curve [19]. As the FD-curves were recorded at five different tip retraction speeds, the adhesion events observed between the virus-CS span over a wide range of LRs, allowing us to probe the dependency of the rupture force on the applied loading rate [20]. Therefore, the extracted data (F and LR for each observed adhesion event) were merged into 6 (WT) or 7 (gCΔmuc) bins of equal LR ranges (**Suppl. Fig. 2**). Within each LR range, the measured rupture forces were displayed as frequency histograms (**Figure 2b** and **Suppl Fig. 3 and 4**) [16], allowing us to determine the most probable rupture forces. The histograms revealed bi- and triGaussian distributions for the WT and the gCΔmuc viruses respectively. These kind of multi-distributions have been previously observed for closely-related multivalent systems where the different peak can either be associated to a single interaction between a viral glycoprotein and a GAG moiety or multiple interactions thereof [16]. The first peak observed at ~50 pN in the histograms is, in both cases, well-above the noise limit and in range with reported single lectin-sugar interactions [13, 21] suggesting that this first peak observed for the WT virus can be attributed to a single interaction recorded between a viral glycoprotein and a CS moiety. The peaks at highest forces result from the simultaneous breaking of multiple virus-CS bonds, as confirmed after applying the William-Evans model [22] to fit the data (**Figure 3b**). A comparison of the histograms (**Figure 2c**) revealed that the measured binding forces were overall higher for the mutant virus lacking the MLR on gC as compared to the wild-type virus, this trend was observed for all the LR ranges (**Suppl. Fig. 5**). The observation of higher binding forces for KOSc-gCΔmuc is in line with the idea that virus release is energetically more demanding in absence of the MLR. [9]

For each virus, we then reported the mean value of each peak observed in the histograms, representing the most probable rupture force for each number of bond, into a dynamic force spectroscopy (DFS) plot (**Figure 3**). The observed linear increase of the rupture forces with the logarithmic loading rate has been described previously for other receptor-ligand systems and explained by the crossing of a single free-energy barrier during the mechanical pulling from the bound to the unbound state [23]. Fitting the data points with the Bell-Evans model[23](**Figure 3a**) allows the kinetic parameters of single bonds to be extracted, including the distance to the transition state (x_β) and the kinetic off rate (k_{off}). The parameters extracted for the WT virus-CS single interaction were x_β = 1.02 ± 0.04 nm and k_{off}= 2.65 x 10^{-4} ± 1.77 x 10^{-4} s^{-1}. Using the Williams-Evans model [22], the binding strength for multiple bonds loaded in parallel can be predicted. For the WT virus, the experimental data were well-described by this prediction (**Figure 3a**), suggesting that in the case of the WT virus, the interactions occurring at higher force and yielding the second peak arise from the multivalent binding of a single type of viral glycoprotein. This multivalency in ligand-receptor bonds is widely observed for viruses [13, 16, 24-25]. Similarly, kinetic parameters of the mutant virus were also extracted yielding the following parameters (**Figure 3b**): x_β = 1.02 ± 0,04 nm and k_{off}= 4.3 x 10^{-5} ± 2.9 x 10^{-5} s^{-1}, indicating that the lifetime of the single bond established between the gCΔmuc virus and CS strongly differs, resulting in a 6 times more stable bond. The Williams-Evans prediction for two simultaneous bonds fits well with the rupture forces observed for the third peaks in the histograms (**Figure 3b**). This suggests that the second component within the histograms arises from another type of interaction, i.e. probably involving another viral glycoprotein. Fitting with the Bell-Evans model yields following parameters for the second interaction: k_{off}= 2.15 x 10^{-6} ± 5.7 x 10^{-6} s^{-1} and x_β = 0.79 ± 0.1nm, resulting therefore in a ~100 times more stable monovalent bond that the one observed for KOSc WT.

Taken together, the *FD*-based AFM data suggests that the presence of the MLR on gC affects the release behavior of HSV-1 from CS by influencing the type of glycoprotein involved in the interaction and the affinity of the individual glycoprotein-GAG interactions. Indeed, the WT virus was found to interact mainly via one type of glycoprotein forming either single or multiple bonds with the surface-immobilized GAGs. This interaction is most likely ascribed to gC which has been proposed to act as main GAG-binding protein [7-8, 26]. This is further confirmed by our control experiments performed with a gC-deficient virus (KOSc-ΔgC) and revealing that other

glycoproteins [27-28] come in play in the absence of gC. (see **Suppl. Fig. 6**). In the case of KOSc-gCΔmuc, it appears that the virus uses at least two distinct glycoproteins characterized by a more stable interaction (k_{off} is decreased by a factor ~6 resp ~100). These glycoprotein-mediated interactions are likely to be ascribe to glycoproteins gCΔmuc and gB [27]. Indeed, we have previously reported that upon deletion of the MLR, purified gCΔmuc proteins still interact with CS via the expected binding site, although dissociation was significantly lower as compared to native gC. [9] Additionally, gB has been shown to serve as a surrogate attachment protein in the absence of gC [27]. However, in this case, it cannot be excluded that glycoprotein D (gD) also binds to CS since this protein interact with specific sequences on HS [29] and co-crystalizes with sulfate ions, implying affinity for sulfated GAG chains [30], although an interaction with CS has not been reported previously.

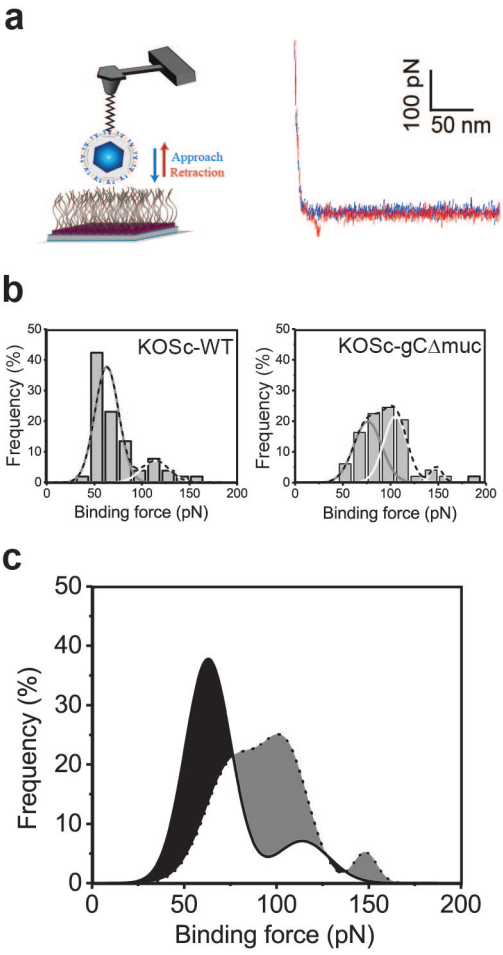

Figure 2: FD-based AFM to probe binding forces of single HSV-1 particles to end-grafted CS chains. a) (left) Illustration of the experimental setup. The AFM tip is coated with one HSV-1

virion using a PEG-linker and follows cycles of approach and retraction to interact with the CS-coated surface. (right) Representative *FD* curve from which the binding forces are extracted. b) Representation of the measured rupture forces as histograms for one discrete LR range (LR 2) and multi-peak Gaussian fitting of the histograms. c) Comparison of overall Gaussian curves fitting rupture forces recorded between CS and KOSc WT or KOSc-gCΔmuc virions. Black-shaded areas show higher binding frequencies for KOSc WT, while the grey-shaded areas correspond to higher binding frequencies for KOSc-gCΔmuc.

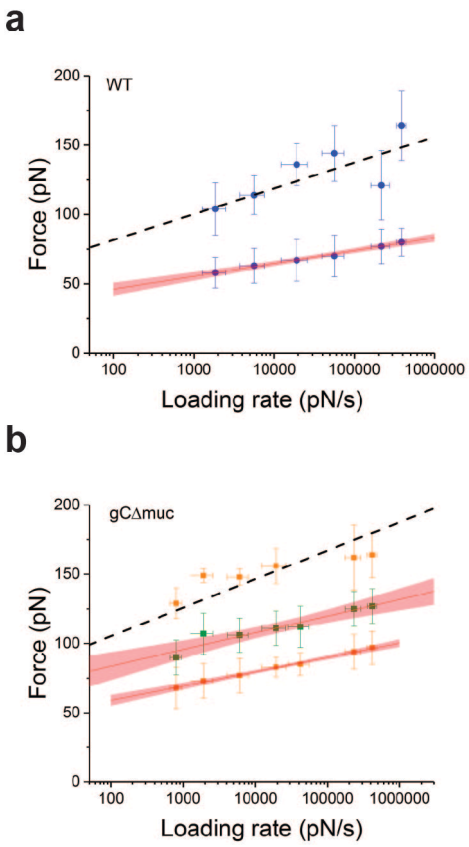

Figure 3: Dynamic force spectroscopy (DFS) plot and extraction of kinetic parameters of virus binding towards CS. a) DFS plot reporting average values of rupture forces for WT virus interacting with CS, allowing analysis with the Bell-Evans model (red line). The dashed line represents the Williams-Evans prediction for the simultaneous rupture of two uncorrelated bonds. b) DFS plot for gCΔmuc virus-CS interactions. Dashed lines represent the Williams-Evans prediction for the rupture of two bonds based on the kinetic parameters calculated from the interaction ruptured at the lowest forces (orange squares, first type of interaction). Green squares

(second interaction type) were fitted with the Bell-Evans model corresponding to a second type of glycoprotein.

Deletion of the MLR on gC affects the accessibility of specific sites on gB, gC and gD

Having found substantial differences in binding strength of CS-bound viruses and in the type of proteins involved in the interaction upon deletion of the MLR on gC, we further tested whether these effects could be related to a change in accessibility to functional sites of the viral glycoproteins. To this end, we used an ELISA-based method to measure the reactivity of monoclonal antibodies with KOSc WT and KOSc-gCΔmuc (**Figure 4**). These tests showed that deletion of the MLR on gC resulted in an increase in accessibility of glycoproteins gB and gD, but a decrease in accessibility of the monoclonal antibody-binding domain on gC partially overlapping with the GAG-binding site [31]. The accessibility of gE appeared similar for both viral strains, confirming that the above-reported differences were not due to a difference in the amount of cell-bound virus. These results therefore suggest that the presence of the MCL-region on gC is two fold. First of all, the MCL-region influences the virus-GAG interaction by enhancing recognition of the GAG by gC. This is in line with the idea that the MCL-region can contribute to specifically exposing GAG-binding sites by influencing the glycoprotein's conformation and by stretching it to enhance the availability of specific sites. [3, 9] In addition to this, the mucin-like domain also shields potential GAG-binding sites on gB. Accordingly, we conclude that the reduced accessibility of the GAG binding site on gC, and the increased accessibility of gB in the absence of the MLR, most likely lead to a preferential involvement of gB in binding to CS for KOSc-gCΔmuc; this could explain the observed increase in binding strength as well as the decrease in virus mobility.

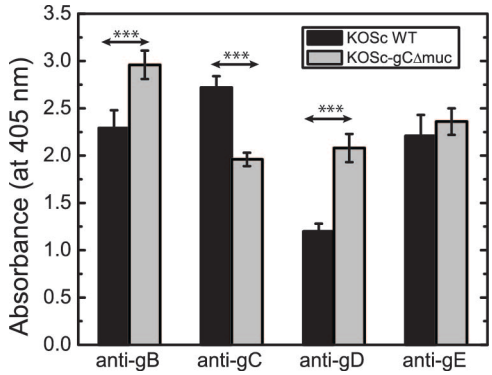

Figure 4: ELISA-based assay to probe the binding of monoclonal antibodies specific to glycoproteins gB, gC, gD, and gE, to cell-bound HSV-1 particles expressing the mucin-like

domain on gC (KOSc WT) or deficient in its expression (KOSc-gCΔmuc). Three separate experiments showing similar differences were performed, and the data presented are means of nine replicates from the last experiment. Significant shifts (***$p<0.001$) are indicated.

Taken together, our results suggest that the MLR on gC plays a major role in balancing the interactions of HSV-1 with the cell membrane during attachment and release: On the one hand, it appears to specifically expose or optimize the accessibility of the GAG-binding site on gC to ensure successful initial attachment to the cell surface. On the other hand, it also shields glycoproteins gB and gD, most likely to regulate the involvement of these molecules, mainly responsible for surrogate attachment and cell entry, respectively [32]. Premature activation of gB could lead to too strong attachment of the virus particle to GAGs, and thereby restrict its lateral mobility. This diffusive behavior could be of importance for the virus during initial attachment to travel through the extracellular matrix rich in GAGs, and along the cell surface to find suitable receptor sites for entry [33]; premature trapping of the virus on the cell surface could therefore hinder successful cell infection. Finally, an unbalanced and too strong interaction of HSV with GAGs and other cell membrane receptors can also lead to trapping of new progeny virus on the surface of infected cells, as observed in our previous study [9], which suggests that the MLR promotes the release of progeny virus from the cell surface. The extent of the contribution of gC for attachment of HSV-1 to cells has long been disputed, in particular in view of the fact that the mutant gC-deficient HSV-1 has been shown capable of binding to and productively infecting the cells [27, 31, 34-35]. Our present data revealed that in wild type HSV-1, glycoprotein gC is a sole component responsible for the virus binding to GAG chains while absence of gC or a deletion of its mucin-like region exposed the GAG-binding capability of gB thus making the gC-altered or the gC-deficient mutants capable of attaching to and infecting the cells.

Since the O-glycans of the gC-1 MLR appear to be directly involved in the balancing of the interactions of HSV-1 with the cell membrane, the possibility that the host itself modulates these processes should not be overlooked. Initiation of O-linked glycosylation of host as well as viral MLRs is carried out by as many as 20 human GalNAc transferase where each of those enzymes has a unique MLR target peptide sequence selectivity and is expressed in a tissue-dependent manner [36-37]. The addition of the initial GalNAc units to the gC-1 MLR is arranged in a complex seed-and spread- manner involving the consecutive actions of at least three sets of different but sequentially operating host GalNAc transferases [38]. This argues for a high degree of qualitative

and quantitative variation in the pattern of O-glycan occupancy of potential gC-1 MLR O-glycosylation sites, solely dependent on which combination of the 20 human GalNAc transferase genes happens to be expressed in the tissue in which HSV-1 replicates. Hence, the involvement of the MLR of HSV-1 gC during viral attachment may be host-cell specific and indeed delicate.

Materials and Methods

Materials – All materials were purchased from commercial sources, unless stated otherwise. 1-palmitoyl-2-oleoyl-sn-glycero-3-phosphocholine (POPC) and 1,2-dioleoyl-sn-glycero-3-phosphoethanolamine-N-(cap bio- tinyl) (sodium salt) (DOPE-biotin) was from Avanti Polar Lipids (Alabaster, AL). Phosphate-buffered saline (PBS, tablets), streptavidin (SA), and PKH26 red fluorescent cell linker kit (containing PKH26 dye and diluent C) were obtained from Sigma-Aldrich (Munich, Germany). Illustra MicroSpin S-200 HR columns were from GE Healthcare (Danderyd, Sweden). Chondroitin sulfate (CS, mixture of 70% chondroitin-4-sulfate(CS-A), and 30% chondroitin-6-sulfate (CS-C)) was purchased from Kraeber (Ellerbek, Germany), and hyaluronan (HA) from Aqua Biochem (Dessau, Germany); both were biotinylated at their reducing end as decribed previously [9, 39].

Virus production and purification – We used the virus strain HSV-1 KOS (VR-1493; ATCC, Manassas, VA) [40] and its variant HSV-1 KOS-gCΔmuc [9, 11], lacking the MLR (amino acids 33-116) in gC. The virus strains were cultured in GMK AH1 cells [41] and purified from the cell culture medium by centrifugation through a three-step discontinuous sucrose gradient [42]. Quantification of the purified virus suspensions was obtained using real-time quantitative PCR of extracted viral DNA [43], and a viral plaque titration assay [42]. These two assays yielded for the purified HSV-1 strain KOSc 1.5×10^{10} PFU/ml and 6.55×10^{10} DNA copies/ml and for the purified HSV-1 mutant virus KOSc-gCΔmuc 2.5×10^{9} PFU/ml and 4.12×10^{10} DNA copies/ml.

AFM tip functionalization – Virus particles were grafted to AFM tips by means of NHS-PEG_{27}-acetal linkers. AFM tips (MSCT probes, Bruker) were immersed in chloroform for 10 min, rinsed with ethanol, dried with a stream of filtered nitrogen, cleaned for 10 min in an ultraviolet radiation and ozone (UV-O) cleaner (Jetlight) and immersed overnight in an ethanolamine solution (3.3 g of ethanolamine hydrochloride in 6.6 mL of DMSO). The cantilevers were then washed three times with DMSO and two times with ethanol, and dried with nitrogen. To ensure a low

grafting density of the linker on the AFM tip, 1 mg of acetal-PEG_{27}-NHS was diluted in 0.5 mL of chloroform with 30 µL of trimethylamine [14]. Ethanolamine-coated cantilevers were immersed for 2 h in this solution, then washed three times with chloroform, and dried with nitrogen. Next, the cantilevers were immersed for 10 min in 1% citric acid in water, washed three times with water and dried with nitrogen. An 80 µL aliquot of either HSV-1 KOSc, HSV-1 KOSc gCΔmuc or HSV-1 KOSc ΔgC (~10^8 particles mL^{-1}) was thawed and centrifuged at 1,677 x g for 1 min to remove aggregates. Besides removing aggregates this gentle centrifugation ensured that the remaining virus solution was highly diluted as needed to bind only a few viruses to the functionalised AFM tip. 70 µL of virus solution were pipetted onto the tips placed on Parafilm (Bemis NA) in a small plastic dish stored within an icebox. 2 µL of a freshly prepared solution of $NaCNBH_3$ (~6% wt. in 0.1 M $NaOH_{(aq)}$) were gently mixed into the virus solution and the cantilever chips gently positioned with their cantilevers extending into the virus drop. The icebox was incubated at 4°C for 1 h. Then, 5 µL of 1 M ethanolamine solution (pH 8) were gently mixed into the drop to quench the reaction. The icebox was incubated for a further 10 min at 4°C, the cantilever chips were removed, washed once in ice-cold PBS, and stored in individual wells of a multiwell dish containing 2 mL of ice-cold PBS per well until used in AFM experiments. During these functionalisation steps the virus-functionalised cantilevers were never allowed to dry. Transfer of the functionalised AFM cantilevers to PBS buffer and then to the AFM was rapid (≤20 s) and during transfer a drop of PBS buffer remained on cantilever and tip. Cantilevers were used in AFM experiments the same day they were functionalised with the virus.

Preparation of GAG-coated surfaces – In preparation for TIRFM experiments, glass cover slides were boiled for >1 h in a 10% 7 × detergent/Milli-Q solution (MP Biomedicals, Santa Ana, CA) and stored in Milli-Q water until use. The glass sides were then rinsed in Milli-Q and dried under N_2 flow. Microwells of ~18 µl were formed using a thin rectangular piece of polydi-methylsiloxane (PDMS). Instead, for the AFM experiments, round glass slides (0.9 mm diameter) were cleaned using a piranha solution (3:1 of H_2SO_4 and 30% of H_2O_2), followed by Milli-Q rinsing, N_2 drying, and 15 min UV-ozone cleaning. The slides were attached to a metal chip using colored reinforcement rings, allowing easy deposition of a ~50 µl drop of solution on top of the glass.

For both TIRFM and AFM experiments, the surfaces were functionalized as described previously [10]. Briefly, supported lipid bilayers (SLBs) were formed on cleaned glasses by

incubating the surface for 20 min with a 0.1 mg/mL solution of POPC + 1 wt % DOPE-biotin vesicles (extruded 11 times through a 30 nm polycarbonate membrane (Whatman) using a mini extruder (Avanti Polar Lipids)). After thorough rinsing with PBS, the surfaces were incubated for 20 min with ~0.25 mg/mL of streptavidin (followed by PBS rinsing) and ~0.5 mg/mL of end-biotinylated CS or ~0.1 mg/mL of end-biotinylated HA (followed by PBS rinsing).

Fluorescent labeling of virus suspensions – The virus suspensions were fluorescently labeled using a PKH26 red fluorescent cell linker kit. 10 µl of virus suspension was mixed with 3 µl of dye (0.5 mM in ethanol) and 200 µl of diluent C, incubated on ice for 10 min, and centrifuged for 2 min at 740 × g using illustra MicroSpin S-200 HR columns.

Single Particle Tracking – 10 µl of fluorescent virus solution was added to ~5 µl of PBS buffer covering the CS-functionalized surfaces. After ~60 min incubation time, time-lapse movies (0.67 fps) were recorded using a Nikon Eclipse Ti-E inverted microscope (Nikon Corporation, Minato, Japan), equipped with a 60× oil immersion objective (NA = 1.49), an Andor DU879E-CSBV camera (Andor Technology, Belfast, UK), an X-Cite 120 light source (Lumen Dynamics Group, Mississauga, Canada), and a TRITC filter cube (Nikon).

The recorded time-lapse movies were analyzed with in-house written MATLAB (The MathWorks, Natick, MA) script for single particle tracking [10]. Briefly, the software detects particles of intensity higher than a set threshold, and builds trajectories using nearest-neighbor linking [44]. For each trajectory, the dependence of mean square displacement (MSD) on lag time (Δt) was calculated using internal averaging [45]. To determine the diffusion mode of the trajectories, the MSD-Δt curves were fitted using both a model for normal, and a model for anomalous diffusion [10]. From these fits, diffusion coefficients (*D* values) were obtained for each trajectory. For each diffusion mode, the software generated histograms of *D* values, which were fitted using log-normal Gaussian fits to determine peak *D* values and calculate mobile fractions (# particles in the mobile peak / # particles assigned to diffusion mode). Combined mobile fractions were calculated as the sum of mobile fractions for normal and anomalous diffusion, weighted by the fraction of particles assigned to each diffusion mode.

***FD*-based AFM –** A Nanoscope Multimode 8 (Bruker) was operated (Nanoscope software v9.1) to conduct FD-based AFM. MSCT-D probes (with calculated spring constants, using thermal tune [46], ranging from 0.029 to 0.056 N m^{-1}) were used to record 5x5 µm arrays, corresponding to

1024 force curvesin the force-volume (contact) mode with an approach velocity of 1 µm s^{-1} and retraction velocities of 0.1, 0.2, 1, 10 and 20 µm s^{-1}, a ramp size of 200 nm, a maximum force of 500 pN and no surface delay. The sample was scanned using a line frequency of 1 Hz and 32 pixels were scanned per line (32 lines). All FD-based AFM measurements were conducted in PBS at ~25°C. For each virus, 3 different experiments were performed, while at least 3 different tips were used in each experiment. Force curves were analysed using the Nanoscope analysis software v1.7 (Bruker). To ensure that the analyzed adhesive peaks correspond to adhesion events occurring between particles linked to the PEG spacer and the heparin surface, the retraction curves before bond rupture were fitted with the worm-like chain model for polymer extension [47] and only events located at least 9 nm (the length of the PEG linker) from the contact point were considered. The latter expresses the force-extension (F-*x*) relationship for semi-flexible polymers and is described by the following equation, with l_P the persistence length and L_c the contour length:

$$F = \frac{k_b T}{l_P}\left(\frac{1}{4\left(1-\frac{x}{L_c}\right)^2}+\frac{x}{L_c}-0.25\right)$$

Origin software (OriginLab) was used to fit histograms of rupture force distributions.

ELISA assay – HSV-1 KOSc WT and HSV-1 KOS-gCΔmuc were added at a moi of 40 (based on the PFU counts) to a monolayer of confluent GMK AH1 cells in 96 well plates at 4°C to prevent cell entry. After 4 h the cells were fixated with 0.25% glutaraldehyde and rinsed with PBS. The reactivity of monoclonal anti-gB (HSV1-B11D8), anti-gC (B1C1B4), anti-gD (C4D5G2), and anti-gE (B1E6A5) was tested using an ELISA-based method, as described previously. [12, 31]

Acknowledgements

The authors acknowledge Stephanie Möller and Matthias Schnabelrauch from INNOVENT e.V., (Jena, Germany) for providing biotinylated CS and HA, Stephan Block (Freie Universität Berlin) for the SPT scripts and Maria Johansson with help with virus purification and the ELISA assay. This work was supported by the Université catholique de Louvain (F.S.R. – Fonds Spéciaux

de Recherche) and the Fonds National de la Recherche Scientifique (FRS-FNRS). M.D. and D.A. are respectively Research Fellow and Research Associate of the FRS-FNRS.

The Swedish Research Council (Vetenskapsrådet, 621-2012-5024 and 2017-04029 to M.B.), and the Area of Advance Materials (Materials for Health, Chalmers) are acknowledged for financial support.

References

1. Datema, R.; Olofsson, S.; Romero, P. A., Inhibitors of protein glycosylation and glycoprotein processing in viral systems. *Pharmacol Ther* **1987,** *33* (2-3), 221-86.
2. Bagdonaite, I.; Wandall, H. H., Global aspects of viral glycosylation. *Glycobiology* **2018,** *28* (7), 443-467.
3. Vigerust, D. J.; Shepherd, V. L., Virus glycosylation: role in virulence and immune interactions. *Trends Microbiol* **2007,** *15* (5), 211-8.
4. Olofsson, S.; Hansen, J. E., Host cell glycosylation of viral glycoproteins--a battlefield for host defence and viral resistance. *Scand J Infect Dis* **1998,** *30* (5), 435-40.
5. Jentoft, N., Why are proteins O-glycosylated? *Trends Biochem Sci* **1990,** *15* (8), 291-4.
6. Olofsson, S., Carbohydrates in Herpesvirus Infections. *Apmis* **1992,** *100*, 84-95.
7. WuDunn, D.; Spear, P. G., Initial interaction of herpes simplex virus with cells is binding to heparan sulfate. *J Virol* **1989,** *63* (1), 52-8.
8. Banfield, B. W.; Leduc, Y.; Esford, L.; Visalli, R. J.; Brandt, C. R.; Tufaro, F., Evidence for an interaction of herpes simplex virus with chondroitin sulfate proteoglycans during infection. *Virology* **1995,** *208* (2), 531-9.
9. Altgarde, N.; Eriksson, C.; Peerboom, N.; Phan-Xuan, T.; Moeller, S.; Schnabelrauch, M.; Svedhem, S.; Trybala, E.; Bergstrom, T.; Bally, M., Mucin-like Region of Herpes Simplex Virus Type 1 Attachment Protein Glycoprotein C (gC) Modulates the Virus-Glycosaminoglycan Interaction. *J Biol Chem* **2015,** *290* (35), 21473-21485.
10. Peerboom, N.; Block, S.; Altgarde, N.; Wahlsten, O.; Moller, S.; Schnabelrauch, M.; Trybala, E.; Bergstrom, T.; Bally, M., Binding Kinetics and Lateral Mobility of HSV-1 on End-Grafted Sulfated Glycosaminoglycans. *Biophys J* **2017,** *113* (6), 1223-1234.
11. Ekblad, M.; Adamiak, B.; Bergefall, K.; Nenonen, H.; Roth, A.; Bergstrom, T.; Ferro, V.; Trybala, E., Molecular basis for resistance of herpes simplex virus type 1 mutants to the sulfated oligosaccharide inhibitor PI-88. *Virology* **2007,** *367* (2), 244-52.
12. Lycke, E.; Johansson, M.; Svennerholm, B.; Lindahl, U., Binding of herpes simplex virus to cellular heparan sulphate, an initial step in the adsorption process. *J Gen Virol* **1991,** *72 (Pt 5)*, 1131-7.
13. Alsteens, D.; Newton, R.; Schubert, R.; Martinez-Martin, D.; Delguste, M.; Roska, B.; Muller, D. J., Nanomechanical mapping of first binding steps of a virus to animal cells. *Nat Nanotechnol* **2017,** *12* (2), 177-183.
14. Wildling, L.; Unterauer, B.; Zhu, R.; Rupprecht, A.; Haselgrubler, T.; Rankl, C.; Ebner, A.; Vater, D.; Pollheimer, P.; Pohl, E. E.; Hinterdorfer, P.; Gruber, H. J., Linking of Sensor Molecules with Amino Groups to Amino-Functionalized AFM Tips. *Bioconjugate Chem* **2011,** *22* (6), 1239-1248.
15. Newton, R.; Delguste, M.; Koehler, M.; Dumitru, A. C.; Laskowski, P. R.; Muller, D. J.; Alsteens, D., Combining confocal and atomic force microscopy to quantify single-virus binding to mammalian cell surfaces. *Nat Protoc* **2017,** *12* (11), 2275-2292.
16. Delguste, M.; Zeippen, C.; Machiels, B.; Mast, J.; Gillet, L.; Alsteens, D., Multivalent binding of herpesvirus to living cells is tightly regulated during infection. *Sci Adv* **2018,** *4* (8), eaat1273.
17. Flory, J. P., *Statistical Mechanics of Chain Molecules*. Hansee: Münich, 1989.
18. Altgarde, N.; Nileback, E.; de Battice, L.; Pashkuleva, I.; Reis, R. L.; Becher, J.; Moller, S.; Schnabelrauch, M.; Svedhem, S., Probing the biofunctionality of biotinylated hyaluronan and chondroitin sulfate by hyaluronidase degradation and aggrecan interaction. *Acta Biomater* **2013,** *9* (9), 8158-66.
19. Alsteens, D.; Tay, S.; Muller, D. J., Toward high-throughput biomechanical phenotyping of single molecules. *Nat Methods* **2015,** *12* (1), 45-6.
20. Merkel, R.; Nassoy, P.; Leung, A.; Ritchie, K.; Evans, E., Energy landscapes of receptor-ligand bonds explored with dynamic force spectroscopy. *Nature* **1999,** *397* (6714), 50-53.

21. Touhami, A.; Hoffmann, B.; Vasella, A.; Denis, F. A.; Dufrene, Y. F., Probing specific lectin-carbohydrate interactions using atomic force microscopy imaging and force measurements. *Langmuir* **2003,** *19* (5), 1745-1751.
22. Evans, E.; Williams, P., *Physics of Bio-Molecules and cells*. Springer: 2002.
23. Evans, E.; Ritchie, K., Dynamic strength of molecular adhesion bonds. *Biophys J* **1997,** *72* (4), 1541-1555.
24. Rankl, C.; Kienberger, F.; Wildling, L.; Wruss, J.; Gruber, H. J.; Blaas, D.; Hinterdorfer, P., Multiple receptors involved in human rhinovirus attachment to live cells. *P Natl Acad Sci USA* **2008,** *105* (46), 17778-17783.
25. Sieben, C.; Kappel, C.; Zhu, R.; Wozniak, A.; Rankl, C.; Hinterdorfer, P.; Grubmuller, H.; Herrmann, A., Influenza virus binds its host cell using multiple dynamic interactions. *P Natl Acad Sci USA* **2012,** *109* (34), 13626-13631.
26. Trybala, E.; Svennerholm, B.; Bergstrom, T.; Olofsson, S.; Jeansson, S.; Goodman, J. L., Herpes simplex virus type 1-induced hemagglutination: glycoprotein C mediates virus binding to erythrocyte surface heparan sulfate. *J Virol* **1993,** *67* (3), 1278-85.
27. Herold, B. C.; Visalli, R. J.; Susmarski, N.; Brandt, C. R.; Spear, P. G., Glycoprotein-C-Independent Binding of Herpes-Simplex Virus to Cells Requires Cell-Surface Heparan-Sulfate and Glycoprotein-B. *Journal of General Virology* **1994,** *75*, 1211-1222.
28. Spear, P. G., Herpes simplex virus: receptors and ligands for cell entry. *Cell Microbiol* **2004,** *6* (5), 401-10.
29. Shukla, D.; Liu, J.; Blaiklock, P.; Shworak, N. W.; Bai, X.; Esko, J. D.; Cohen, G. H.; Eisenberg, R. J.; Rosenberg, R. D.; Spear, P. G., A novel role for 3-O-sulfated heparan sulfate in herpes simplex virus 1 entry. *Cell* **1999,** *99* (1), 13-22.
30. Carfi, A.; Gong, H. Y.; Lou, H.; Willis, S. H.; Cohen, G. H.; Eisenberg, R. J.; Wiley, D. C., Crystallization and preliminary diffraction studies of the ectodomain of the envelope glycoprotein D from herpes simplex virus 1 alone and in complex with the ectodomain of the human receptor HveA. *Acta Crystallogr D* **2002,** *58*, 836-838.
31. Trybala, E.; Bergstrom, T.; Svennerholm, B.; Jeansson, S.; Glorioso, J. C.; Olofsson, S., Localization of a functional site on herpes simplex virus type 1 glycoprotein C involved in binding to cell surface heparan sulphate. *J Gen Virol* **1994,** *75 (Pt 4)*, 743-52.
32. Atanasiu, D.; Saw, W. T.; Cohen, G. H.; Eisenberg, R. J., Cascade of events governing cell-cell fusion induced by herpes simplex virus glycoproteins gD, gH/gL, and gB. *J Virol* **2010,** *84* (23), 12292-9.
33. Boulant, S.; Stanifer, M.; Lozach, P. Y., Dynamics of Virus-Receptor Interactions in Virus Binding, Signaling, and Endocytosis. *Viruses-Basel* **2015,** *7* (6), 2794-2815.
34. Langeland, N.; Oyan, A. M.; Marsden, H. S.; Cross, A.; Glorioso, J. C.; Moore, L. J.; Haarr, L., Localization on the herpes simplex virus type 1 genome of a region encoding proteins involved in adsorption to the cellular receptor. *J Virol* **1990,** *64* (3), 1271-7.
35. Griffiths, A.; Renfrey, S.; Minson, T., Glycoprotein C-deficient mutants of two strains of herpes simplex virus type 1 exhibit unaltered adsorption characteristics on polarized or non-polarized cells. *J Gen Virol* **1998,** *79 (Pt 4)*, 807-12.
36. Bennett, E. P.; Mandel, U.; Clausen, H.; Gerken, T. A.; Fritz, T. A.; Tabak, L. A., Control of mucin-type O-glycosylation: a classification of the polypeptide GalNAc-transferase gene family. *Glycobiology* **2012,** *22* (6), 736-56.
37. Olofsson, S.; Blixt, O.; Bergstrom, T.; Frank, M.; Wandall, H. H., Viral O-GalNAc peptide epitopes: a novel potential target in viral envelope glycoproteins. *Rev Med Virol* **2016,** *26* (1), 34-48.
38. Norden, R.; Halim, A.; Nystrom, K.; Bennett, E. P.; Mandel, U.; Olofsson, S.; Nilsson, J.; Larson, G., O-linked glycosylation of the mucin domain of the herpes simplex virus type 1-specific glycoprotein gC-1 is temporally regulated in a seed-and-spread manner. *J Biol Chem* **2015,** *290* (8), 5078-91.
39. Altgarde, N.; Nileback, E.; de Battice, L.; Pashkuleva, I.; Reis, R. L.; Becher, J.; Moller, S.; Schnabelrauch, M.; Svedhem, S., Probing the biofunctionality of biotinylated hyaluronan and chondroitin sulfate by hyaluronidase degradation and aggrecan interaction. *Acta Biomaterialia* **2013,** *9* (9), 8158-8166.
40. Smith, K. O., Relationship between the Envelope and the Infectivity of Herpes Simplex Virus. *Proc Soc Exp Biol Med* **1964,** *115*, 814-6.
41. Guenalp, A., Growth and Cytopathic Effect of Rubella Virus in a Line of Green Monkey Kidney Cells. *Proc Soc Exp Biol Med* **1965,** *118*, 85-90.
42. Trybala, E.; Liljeqvist, J. A.; Svennerholm, B.; Bergstrom, T., Herpes simplex virus types 1 and 2 differ in their interaction with heparan sulfate. *J Virol* **2000,** *74* (19), 9106-14.
43. Namvar, L.; Olofsson, S.; Bergstrom, T.; Lindh, M., Detection and typing of Herpes Simplex virus (HSV) in mucocutaneous samples by TaqMan PCR targeting a gB segment homologous for HSV types 1 and 2. *J Clin Microbiol* **2005,** *43* (5), 2058-64.

44. Meijering, E.; Dzyubachyk, O.; Smal, I., Methods for Cell and Particle Tracking. *Method Enzymol* **2012,** *504*, 183-200.
45. Saxton, M. J., Single-particle tracking: the distribution of diffusion coefficients. *Biophys J* **1997,** *72* (4), 1744-53.
46. Butt, H. J.; Jaschke, M., Calculation of Thermal Noise in Atomic-Force Microscopy. *Nanotechnology* **1995,** *6* (1), 1-7.
47. Bustamante, C.; Marko, J. F.; Siggia, E. D.; Smith, S., Entropic Elasticity of Lambda-Phage DNA. *Science* **1994,** *265* (5178), 1599-1600.

Graphical table of contents